Boundary-Layer Meteorol (2013) 149:277–301
DOI 10.1007/s10546-013-9839-5

ARTICLE

Surface Heterogeneity Effects on Regional-Scale Fluxes in the Stable Boundary Layer: Aerodynamic Roughness Length Transitions

Nathan E. Miller · Rob Stoll

Received: 2 November 2012 / Accepted: 4 July 2013 / Published online: 31 July 2013

Abstract The effects of abrupt streamwise transitions of the aerodynamic roughness length (z_o) on the stable atmospheric boundary layer are evaluated using a series of large-eddy simulations based on the first Global Energy and Water Cycle Experiment Atmospheric Boundary Layer intercomparison study (GABLS1). Four z_o values spanning three orders of magnitude are used to create all possible binary distributions with each arranged into patches of characteristic length scales equal to roughly one-half, one, and two times the equivalent homogeneous boundary-layer height. The impact of the heterogeneity on mean profiles of wind speed and temperature, on surface fluxes of heat and momentum, and on internal boundary-layer dynamics are considered. It is found that z_o transitions do not significantly alter the functional relationship between the average surface fluxes and the mean profiles of wind speed and potential temperature. Although this suggests that bulk similarity theory is applicable for modelling the stable boundary layer over z_o heterogeneity, effective surface parameters must still be specified. Existing models that solve for effective roughness lengths of momentum and heat are evaluated and compared to values derived from the simulation data. The existing models are unable to accurately reproduce both the values of the effective aerodynamic roughness lengths and their trends as functions of patch length scale and stability. A new model for the effective aerodynamic roughness length is developed to exploit the benefits of the other models tested. It accurately accounts for the effects of the heterogeneity and stratification on the blending height and effective aerodynamic roughness length. The new model provides improved average surface fluxes when used with bulk similarity.

Keywords Aerodynamic roughness length · Blending height · Effective aerodynamic roughness length · Large-eddy simulation · Stable boundary layer · Surface heterogeneity

N. E. Miller · R. Stoll (✉)
Department of Mechanical Engineering, University of Utah, Salt Lake City, UT, USA
e-mail: rstoll2@gmail.com; rstoll@eng.utah.edu

N. E. Miller
e-mail: nmiller@eng.utah.edu

1 Introduction

The dynamic two-way interaction between the atmosphere and the land surface plays a pivotal role in determining fluxes of momentum, heat, and moisture. These fluxes are key components of the hydrologic cycle and must be specified as boundary conditions in regional weather, climate, and hydrologic numerical models. Model predictions are strongly affected by how these boundary conditions are formulated (Viterbo et al. 1999; Holtslag 2006; King et al. 2001, 2007), and this is complicated by two important factors: the complexity of natural land surfaces and the non-linear relationship between turbulence in the atmospheric boundary layer (ABL) and the local vertical fluxes (Brutsaert 1998). In the stable boundary layer (SBL), this is particularly problematic due to small surface fluxes leading to weak turbulent mixing and even intermittent turbulence (Mahrt 1987, 2000; King et al. 2001; Mahrt and Mills 2009).

Researchers have recognized the importance of the role that land-surface heterogeneity plays in land-atmosphere coupling and, as a result, have given it considerable attention (e.g., Mahrt 1987; Avissar and Schmidt 1998; Albertson and Parlange 1999; Roy and Avissar 2000; Bou-Zeid et al. 2007; McCabe and Brown 2007; Stoll and Porté-Agel 2009; Huang and Margulis 2010). A majority of these efforts have focused on daytime convective conditions or the neutral ABL while the nocturnal SBL has received less attention (Fernando and Well 2010). Though several parametrizations have been presented to account for surface heterogeneity, the majority have been developed using convective or neutral conditions (e.g., Avissar and Pielke 1989; Claussen 1990, 1991; Blyth 1995; Bou-Zeid et al. 2007; Huang and Margulis 2010). During the night, when the effect of stratification on local turbulence complicates the relationship between land-surface properties and ABL dynamics, these formulations, which rely on assumptions of the existence of a constant-flux layer and/or a well-defined blending height, are questionable. Recently, Stoll and Porté-Agel (2009) for the first time developed a surface-flux model specifically for the heterogeneous SBL. They used a local scaling hypothesis (Nieuwstadt 1984) to improve the representation of fluxes over patches with different surface temperatures.

Many studies of surface heterogeneity and its effects on the ABL have focused on heterogeneous aerodynamic roughness length (z_o) distributions (e.g., Mason 1988; Claussen 1990; Wood and Mason 1991; Derbyshire 1995; Hopwood 1995; Albertson and Parlange 1999; Goode and Belcher 1999; Lin and Glendening 2002; Bou-Zeid et al. 2004, 2007; Stoll and Porté-Agel 2006a). Even though stable stratification can have an important role in large-scale atmospheric model predictions (Mahrt 1987; Viterbo et al. 1999) and is prevalent at night over land, only a few of these studies included stably stratified ABL conditions (Wood and Mason 1991; Derbyshire 1995). Derbyshire's (1995) experimental work remains one of the few studies to focus on z_o distributions in the SBL.

Here, three-dimensional numerical simulations are used to examine the effects of aerodynamic roughness length heterogeneity on the vertical fluxes of heat and momentum in the SBL, and how flux aggregation methods used as surface boundary conditions in large-scale numerical models reproduce these fluxes. The paper is organized as follows: first, common techniques used to account for aerodynamic roughness length heterogeneity are reviewed. Then, after a brief description of the numerical code used in this study, the numerical simulation data are utilized to examine the resulting boundary-layer structure and to investigate the performance of flux aggregation models. Emphasis is placed on the evaluation of effective roughness length models for momentum and heat transport.

1.1 Effective Aerodynamic Roughness Length Parametrizations

Monin–Obukhov similarity theory (Monin and Obukhov 1954) relates the average wind speed and the potential temperature difference across the surface layer with the surface fluxes. It forms the basis of almost all surface-flux parametrizations. In the ABL, Monin–Obukhov similarity theory can be used to model the mean surface shear stress and heat flux as:

$$\langle \tau_s \rangle = \left[\frac{\langle M(Z_m) \rangle \kappa}{\ln \left(Z_m / z_{o,e} \right) - \Psi_m} \right]^2, \tag{1}$$

$$\langle H_s \rangle = -\frac{u_* \left[\langle \theta(Z_m) \rangle - \theta_s \right] \kappa}{\ln \left(Z_m / z_{t,e} \right) - \Psi_h}, \tag{2}$$

where $\langle \tau_s \rangle$ is the mean surface shear-stress magnitude, $\langle \tau \rangle = \sqrt{\langle u'w' \rangle^2 + \langle v'w' \rangle^2}$ (where u, v, and w are the streamwise, spanwise, and surface normal components of the velocity and the prime denotes a fluctuation from the horizontal mean), $\langle H_s \rangle$ is the surface value of the mean heat flux $\langle H \rangle = \langle w'\theta' \rangle$, $\langle M \rangle = \sqrt{\langle u \rangle^2 + \langle v \rangle^2}$ is the mean wind speed, θ is the potential temperature, $u_* = \sqrt{\langle \tau_s \rangle}$ is the surface friction velocity, κ is the von Kármán constant (= 0.4), Z_m is a reference height, Ψ_m and Ψ_h are stability functions (see Garratt 1992, for details), $\langle\ \rangle$ represents a spatial average, and the subscript s denotes a surface value. The variables $z_{o,e}$ and $z_{t,e}$ are usually referred to as the effective roughness lengths for momentum and heat, respectively (Mason 1988; Claussen 1990; Mahrt 1996). In the case of a homogeneous surface temperature θ_s, modelling the surface flux over heterogeneous terrain can be simplified to specifying $z_{o,e}$ and $z_{t,e}$. Here, the focus is on examining how to specify these parameters. This approach to surface-flux modelling for roughness length heterogeneity is distinctly different than approaches used to model fluxes over heterogeneous temperature transitions. This latter case is discussed in detail in Stoll and Porté-Agel (2009).

The goal in defining effective roughness length parameters is either to predict the correct mean velocity and temperature profiles (Taylor 1987) or to predict the correct average surface stress and flux (Mason 1988; Claussen 1990, 1991; Wood and Mason 1991; Beljaars and Holtslag 1991). These effective parameters are then used with Eqs. 1 and 2 to estimate the area-averaged surface stress and flux.

Taylor (1987) developed a simple estimate for $z_{o,e}$ based on the logarithmic velocity law, the assumption that the flow is in vertical equilibrium everywhere, and the assumption that local changes in the surface stress due to aerodynamic roughness length transitions are minimal,

$$\ln(z_{o,e}) = \frac{1}{n} \sum_{i}^{n} \ln(z_{o,i}), \tag{3}$$

where n is the total number of local aerodynamic roughness length values $z_{o,i}$.

An alternative method developed to estimate effective parameters uses the idea that the flow becomes approximately homogeneous at a vertical scale termed the 'blending height' (Wieringa 1986; Mason 1988; Claussen 1990, 1991; Wood and Mason 1991; Mahrt 1996; Brutsaert 1998). Two different definitions for the blending height are prevalent in the literature. The first defines the blending height as the height at which the mean velocity and temperature profiles are approximately in equilibrium with the surface (Mason 1988; Wood and Mason 1991). The second common definition is the height at which the flow is everywhere in equilibrium with the surface (Claussen 1990, 1991). This height is typically an order of magnitude greater than that of the first definition (Schmid and Bünzli 1995). With the first definition, Mason (1988) uses the assumption that horizontal advection balances the vertical stress divergence to give the following estimate for the blending height for momentum h_b in a neutrally stratified ABL,

$$h_\mathrm{b}\left[\ln\left(\frac{h_\mathrm{b}}{z_\mathrm{o,e}}\right)\right]^2 = 2\kappa^2 L_\mathrm{c}, \tag{4}$$

where L_c is the length scale of horizontal variation. For well-defined surface heterogeneity (e.g., streamwise patches) L_c is simple to identify. In the general case, second-order structure functions of the aerodynamic roughness length distribution can be used to define L_c (Bou-Zeid et al. 2007). In stably stratified flows, Wood and Mason (1991) recommends that the definition of h_b should be modified to include stability corrections. This requires the use of an effective Obukhov length ($L_\mathrm{e} = -\theta_\mathrm{r}\langle\tau_\mathrm{s}\rangle^{3/2}\,(g\kappa\langle H_\mathrm{s}\rangle)^{-1}$, where θ_r is a reference temperature and g is the acceleration due to gravity) defined over the grid cell. Wood and Mason (1991) also calculates a separate blending height for heat ($h_\mathrm{b,h}$) and $z_\mathrm{t,e}$ using a relationship equivalent to that used for h_b and $z_\mathrm{o,e}$, and found that for their tested stability range, $h_\mathrm{b,h}$ has a similar value to h_b. Consequently, in practice many researchers do not advocate any distinction between the blending height for momentum and scalars (Blyth et al. 1993; Blyth 1995; Arola 1999; Ament and Simmer 2006). Bou-Zeid et al. (2007) argue that the aerodynamic roughness length is a property of the surface geometry and therefore, by extension, the effective aerodynamic roughness length should not change with stability.

The second blending height definition is analogous to the diffusion height scale. Claussen (1990) gives the following relationship,

$$h_\mathrm{b}\left[\ln\left(\frac{h_\mathrm{b}}{z_\mathrm{o,e}}\right)\right] = c_1\kappa L_\mathrm{c}, \tag{5}$$

where c_1 is an $O(1)$ constant. Equation 5 is obtained by minimizing the error associated with the assumptions of homogeneity and equilibrium. A similar relationship is derived in Bou-Zeid et al. (2004). They combine empirical large-eddy simulation (LES) data from neutral boundary-layer simulations over aerodynamic roughness length transitions with theoretical equations derived by assuming a balance between vertical diffusion and horizontal advection to obtain,

$$h_\mathrm{b}\left[\ln\left(\frac{h_\mathrm{b}}{z_\mathrm{o,e}}\right) - 1\right] = c_1\kappa(2L_\mathrm{c}), \tag{6}$$

where c_1 is again an $O(1)$ constant that must include, at least in part, the ratio of the root-mean-square of the vertical velocity (w_rms) to u_*, and $2L_\mathrm{c}$ is the approximate downstream distance at which the internal boundary layer (IBL) reaches the blending height. The model developed in Bou-Zeid et al. (2004) as described by Eqs. 6 and 7 (described below) will be referred to as BZ04 from here on.

To determine the blending height using one of Eqs. 4–6, a second relationship between $z_\mathrm{o,e}$ and h_b is required. An iterative procedure must then be employed to solve for both values simultaneously. By assuming that the flow at the blending height is horizontally homogeneous and in equilibrium with the average surface stress, Mason (1988) showed that,

$$\left[\ln\left(\frac{h_\mathrm{b}}{z_\mathrm{o,e}}\right)\right]^{-2} = \sum_i f_i\left[\ln\left(\frac{h_\mathrm{b}}{z_{\mathrm{o},i}}\right)\right]^{-2}, \tag{7}$$

where f_i is the fraction of the total surface area associated with $z_{o,i}$. To include the effect of stratification, Wood and Mason (1991) added stability corrections to Eq. 7.

$$\left[\ln\left(\frac{h_b}{z_{o,e}}\right) - \Psi_m\left(\frac{h_b}{L_e}\right)\right]^{-2} = \sum_i f_i \left[\ln\left(\frac{h_b}{z_{o,i}}\right) - \Psi_m\left(\frac{h_b}{L_i}\right)\right]^{-2}, \tag{8}$$

where L_i is the Obukhov length for an individual area associated with $z_{o,i}$. In order to solve for $h_{b,h}$ and $z_{t,e}$, Wood and Mason (1991) developed another relationship similar to Eq. 8. This was done by equating two relations for $\theta(h_{b,h}) - \langle\theta_s\rangle$ based on the temperature profile created from effective aerodynamic roughness length values and on the average of the local temperature profiles,

$$\frac{\langle H_s\rangle}{\langle\tau_s\rangle^{\frac{1}{2}}}\left[\ln\left(\frac{h_{b,h}}{z_{t,e}}\right) - \Psi_h\left(\frac{h_{b,h}}{L_e}\right)\right] = \sum_i f_i \frac{\langle H_s\rangle_i}{\langle\tau_s\rangle_i^{\frac{1}{2}}}\left[\ln\left(\frac{h_{b,h}}{z_{t,i}}\right) - \Psi_h\left(\frac{h_{b,h}}{L_i}\right)\right], \tag{9}$$

where $\langle\ \rangle_i$ represents a spatial average over an individual area associated with $z_{o,i}$, and $z_{t,i}$ is the roughness length for heat of that same area. The model developed in Wood and Mason (1991) will be referred to as WM91 from here on.

Few authors besides Wood and Mason (1991) use a separate calculation for the effective roughness length for heat. Instead they argue that if $z_{t,e}$ is needed, it should be a function of $z_{o,e}$, similar to the treatment of the roughness length for heat in the homogeneous boundary layer (Claussen 1991; Blyth et al. 1993; Blyth 1995; Arola 1999). In the homogeneous ABL, for continuous vegetation or semi-porous media, z_t is defined as a fraction of z_o. For homogeneously distributed bluff roughness elements, z_t is also a function of the surface friction velocity (Brutsaert 1982; Claussen 1991). It is important to note that most authors recommend calculating the surface heat flux individually over different patches or land-cover types in the heterogeneous ABL (e.g., Avissar and Pielke 1989; Claussen 1991; Blyth et al. 1993; Blyth 1995; Arola 1999; Ament and Simmer 2006). Stoll and Porté-Agel (2009) give a detailed review of the different methods and issues involved with surface heat-flux calculations. Because the surface heat flux is usually calculated locally and then averaged, $z_{t,e}$ is not widely used.

2 Numerical Simulation

The LES model used in this study is described in detail in Stoll and Porté-Agel (2006a, 2008). It solves the filtered conservation of momentum for a Bousinesq fluid in rotational form (Orszag and Pao 1974) and the filtered conservation of heat. Molecular diffusion and dissipation are ignored due to the high Reynolds number in the ABL.

The numerical details of the code can be summarized as follows: spectral methods are used to represent horizontal derivatives and centred differences to calculate vertical derivatives. Time advancement is carried out with a second-order Adams-Bashforth scheme and the convective terms are de-aliased using the 3/2 rule (Canuto et al. 1988). Subgrid-scale (SGS) physics are modelled using a dynamic procedure that is specifically tailored to heterogeneous ABL flows (Stoll and Porté-Agel 2006a). This SGS model has been shown to improve SGS stress and flux calculations in homogeneous and heterogeneous SBL flows (Stoll and Porté-Agel 2008, 2009). The lateral boundary conditions are assumed to be periodic and the boundary conditions at the top of the domain are zero stress (zero vertical velocity) and constant potential temperature gradient. Boundary conditions at the land surface require the specification of the instantaneous filtered surface shear stress and heat flux as functions of the resolved velocity at the lowest computational level and the difference between the surface temperature and the resolved potential temperature at the lowest computational grid level. This is accomplished through the local application of Monin–Obukhov similarity theory. Although Monin–Obukhov similarity theory is strictly only valid for steady homogeneous flows, it is widely used in surface boundary conditions for LES over heterogeneous terrain (e.g., Albertson et al. 2001; Bou-Zeid et al. 2004, 2007; Patton et al. 2005; Stoll and Porté-Agel 2006a, 2009; Huang and Margulis 2010).

2.1 Simulation Set-Up

The simulation set-up for the heterogeneous z_o distribution cases is similar to that used in Stoll and Porté-Agel (2008, 2009). The cases are based on the first GEWEX (Global Energy and Water Cycle Experiment) ABL (GABLS1) LES intercomparison study of Beare et al. (2006). The intercomparison case can be characterized as a moderately stable, continuously turbulent, boundary layer. The boundary layer is driven in the streamwise direction by a geostrophic wind $U_g = 8.0$ m s^{-1}; Coriolis forces act only in the horizontal directions with a Coriolis parameter $f_c = 1.39\times 10^{-4}$ s^{-1}. The simulations are initialized with a constant streamwise velocity magnitude of 8.0 m s^{-1} and zero velocity in the spanwise and surface-normal components. The potential temperature is initialized with a constant value up to a height of 100 m. Above 100 m a constant lapse rate of 0.01 K m^{-1} is prescribed and the surface is cooled homogeneously at a constant rate of 0.25 K h^{-1} throughout the simulation. Each simulation has a duration of nine physical hours with statistics calculated over the last 1 h. The domain has a vertical extent of 400 m and a horizontal span of 800 m in both the streamwise and spanwise directions. This horizontal domain length is twice the original GABLS1 case; the domain was expanded to allow for a larger range of heterogeneous patch length scales. Previous studies have found that simulations with this domain size produce mean profiles of first- and second-order statistics that are indistinguishable from the original 400 m domain (Beare and MacVean 2004; Stoll and Porté-Agel 2008). For all simulations the domain is discretized using $192 \times 192 \times 192$ points in the streamwise, spanwise, and vertical directions, respectively, resulting in a numerical spacing of 2.094 m in the vertical direction and 4.167 m in the horizontal directions. Identical simulations were also run with the domain discretized with $128 \times 128 \times 128$ points (not shown). Grid resolution had a minimal impact on the statistics reported below.

The surface heterogeneity consists of abrupt transitions of roughness lengths of both momentum and heat in the streamwise direction. Four aerodynamic roughness length values spanning a range of three decades are used in binary distributions: 10^{-1}, 10^{-2}, 10^{-3}, and 10^{-4} m. Six different roughness jump combinations are created from the four roughness length values, and each combination is tested with three different patch sizes, 100, 200, and 400 m. The 18 resulting cases all have the rougher surface, $z_{o,1}$, as the foremost streamwise patch. In addition, as a result of the periodic streamwise boundary condition, the patches repeat infinitely in the streamwise direction. Besides the heterogeneous simulations, homogeneous simulations are run with each of the four roughness length values. These simulations establish a reference with which to evaluate the heterogeneous simulations. Simulation based studies often set the roughness length for heat (z_t) as a function of z_o (e.g., Huang and Margulis 2010). Here $z_t = z_o$ at all locations following the convention of the original GABLS1 case (Beare et al. 2006). This formulation is acceptable when the surface temperature is also specified, as it is here, but is questionable when the surface temperature is determined using a surface energy budget.

3 Boundary-Layer Structure from LES

Here we present results from first the homogeneous and then the heterogeneous aerodynamic roughness length simulations described in Sect. 2.1. In the following sections, both one-dimensional horizontal plane-averaged and two-dimensional spanwise-averaged values of first- and second-order statistics are given. The fluctuating values of filtered velocity and temperature required to calculate turbulence statistics are defined as the deviations from the horizontal plane averages. The homogeneous cases are used to establish the response of the simulated SBL to different aerodynamic roughness length values and the heterogeneous cases are examined for the signature of heterogeneous aerodynamic roughness length patches on boundary-layer statistics. The presented results are time averaged over the last 1 h of simulation time (hours 8–9) when the SBL becomes quasi-steady (Beare et al. 2006).

3.1 Homogeneous Aerodynamic Roughness Length Simulations

Before examining the effect of heterogeneous aerodynamic roughness length distributions on fluxes in the SBL, it is important to establish how the boundary layer responds to different z_o values in the homogeneous case. In this section, bulk boundary-layer parameters and mean profiles of wind speed and potential temperature are presented for simulations with the four different values of z_o ranging from 10^{-1} to 10^{-4} m. Table 1 gives the average boundary-layer characteristics from the four homogeneous simulations including the boundary-layer height δ, defined as 1.0/0.95 times the height where the mean stress reaches 5 % of its surface value (Kosovic and Curry 2000), friction velocity u_*, surface temperature scale $\theta_* = -\langle H_s \rangle u_*^{-1}$, and the Obukhov length L.

From Table 1, one of the main effects of reducing z_o can be observed. Reducing z_o decreases the overall surface drag and the transport of momentum and heat at the surface. Over the range of values tested here (three orders of magnitude), the average surface shear-stress magnitude is reduced by approximately 53 % and the surface heat flux by 45 %. The corresponding reduction in boundary-layer height is clearly evident in the wind-speed and potential temperature profiles shown in Fig. 1. In addition to the reduction in the boundary-layer height, surface shear-stress magnitude, and surface heat flux, the boundary layer becomes increasingly stratified as z_o is reduced with the bulk boundary-layer stability parameter δL^{-1} increasing from 1.58 to 1.88 as z_o varies from 10^{-1} to 10^{-4} m.

All the wind-speed profiles in Fig. 1a exhibit elevated wind-speed maxima just below δ in accordance with Nieuwstadt's theoretical model (Nieuwstadt 1984, 1985) and previous LES studies (Kosovic and Curry 2000; Beare and MacVean 2004; Beare et al. 2006; Stoll and Porté-Agel 2008). Although δ, and thus the location of the wind-speed maximum, is altered by changing z_o, the value of the maximum is not. The potential temperature profiles shown

Table 1 Mean boundary-layer characteristics for homogeneous stable boundary-layer simulations with different aerodynamic roughness length values

z_o (m)	Symbol	Linestyle	δ (m)	u_* (m s^{-1})	θ_* (K)	L (m)
10^{-1}	$+$	——	180	0.269	0.0428	114
10^{-2}	$*$	$-\cdot-$	160	0.238	0.0397	96
10^{-3}	♦	......	144	0.210	0.0366	81
10^{-4}	$\times$	$---$	130	0.186	0.0337	69

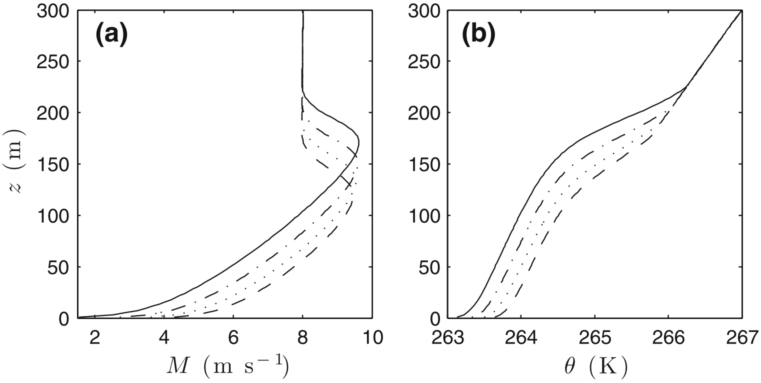

Fig. 1 Mean profiles of wind speed (**a**) and potential temperature (**b**) from the homogeneous SBL with different aerodynamic roughness length values. The profiles are averaged over the last 1 h of simulation time. The *linestyle* definitions are given in Table 1

in Fig. 1b have a similar behaviour. The profiles all shift downwards with δ in Table 1. For all the cases, the temperature profiles also exhibit positive curvature ($\partial^2\theta/\partial z^2 > 0$) within the boundary layer in agreement with Nieuwstadt's model (Nieuwstadt 1984, 1985).

The momentum flux ($\langle\tau\rangle$) in the boundary layer decreases with decreasing z_o with its surface value ranging from 0.072 to 0.035 m^2 s^{-2}. Throughout the boundary layer the momentum-flux profiles have nearly identical curvature (not shown). When normalized by their surface values they all approximately follow a 3/2 power law with $z\delta^{-1}$ in agreement with Nieuwstadt's local scaling hypothesis (Nieuwstadt 1984, 1985). The buoyancy flux ($g\theta_r^{-1}\langle H\rangle$) also decreases in magnitude with decreases in z_o with its surface value varying from a maximum magnitude of -2.5×10^{-2} K m s^{-1} to a minimum magnitude of -1.3×10^{-2} K m s^{-1}. The buoyancy flux has a near-linear profile throughout much of the boundary layer for all tested z_o values (not shown), thus agreeing with the local scaling hypothesis.

The mean velocity, temperature, momentum-flux, and buoyancy-flux profiles are all helpful when assessing the effect of different z_o values throughout the entire SBL. To focus on the near-surface region, we examine the non-dimensional gradients of wind shear and potential temperature. Besides providing a more detailed description of the LES mean velocity and potential temperature profiles near the surface, these gradients form the basis for Eqs. 1 and 2, and are important for surface-layer modelling in large-scale models (e.g., Beljaars and Holtslag 1991; Brutsaert 1998; King et al. 2001). The gradients are defined as,

$$\Phi_M = \left(\frac{\kappa z}{u_*}\right)\sqrt{\left(\frac{\partial\langle u\rangle}{\partial z}\right)^2 + \left(\frac{\partial\langle v\rangle}{\partial z}\right)^2} \tag{10}$$

and

$$\Phi_H = \left(\frac{\kappa z}{\theta_*}\right)\frac{\partial\langle\theta\rangle}{\partial z}. \tag{11}$$

Often these gradients are parametrized as linear functions of the surface-layer stability parameter zL^{-1} as (Businger et al. 1971; Garratt 1992; Arya 2001),

$$\Phi_M = 1 + \gamma_m\frac{z}{L} \tag{12}$$

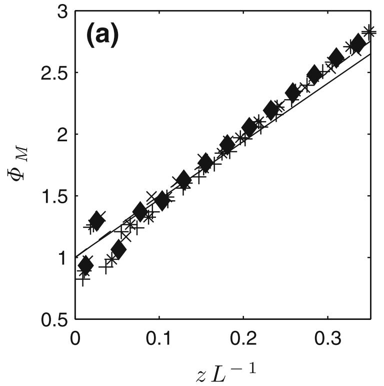

Fig. 2 Non-dimensional velocity gradient (**a**) and potential temperature gradient (**b**) as a function of zL^{-1} in the lowest 40 m of the domain from homogeneous SBL simulations. The formulations given as Eqs. 12 and 13 are shown as the *lines* in the two plots respectively. The *solid lines* use $\gamma_\mathrm{m} = \gamma_\mathrm{h} = 4.7$. The *dashed lines* use $\gamma_\mathrm{m} = \gamma_\mathrm{h} = 5.0$. The *symbol* definitions are given in Table 1

and

$$\Phi_\mathrm{H} = \alpha + \gamma_\mathrm{h}\frac{z}{L}, \tag{13}$$

with the constants having typical values of $\alpha = 0.74$, and $\gamma_\mathrm{m} = \gamma_\mathrm{h}$ between 4.5 and 5.0 (Businger et al. 1971; Dyer 1974; Grachev et al. 2005).

The formulations given by these equations are plotted along with the Φ_M and Φ_H values from the four homogeneous simulations in Fig. 2 as functions of zL^{-1}. The points are all from the lowest 40 m of the simulation domain. Equations 12 and 13 are shown with γ_m and γ_h equal to both 4.7 and 5.0. All four simulations result in non-dimensional velocity and temperature gradients that agree with Eqs. 12 and 13 showing that the change in z_o does not change the functional relationship between the normalized gradients and the stability parameters in homogeneous SBL simulations. Both Φ_M and Φ_H appear to follow the lines using $\gamma_\mathrm{m} = \gamma_\mathrm{h} = 5.0$. Note that the oscillations for near-neutral conditions in Φ_M are a result of the surface boundary condition and have minimal impact on flow statistics above the lowest computational levels (Stoll and Porté-Agel 2006b). This phenomenon is observed in many LES studies of the ABL (e.g., Andrén et al. 1994; Bou-Zeid et al. 2004; Stoll and Porté-Agel 2008).

3.2 Heterogeneous Aerodynamic Roughness Length Simulations

Surface heterogeneity can have a strong impact on the dynamics of the SBL (Stoll and Porté-Agel 2009). This impact must be parametrized in large-scale numerical models of the atmosphere. In this section, the effect of heterogeneous aerodynamic roughness length distributions on the dynamics of the SBL is explored. One-dimensional horizontal plane averages and two-dimensional spanwise-averaged statistics are presented to elucidate the response of the boundary layer to streamwise transitions in z_o. The bulk boundary-layer statistics for each of the 18 simulations, including δ, u_*, θ_*, L, and the ratio of equilibrium stresses over the patches are given in Table 2.

Table 2 Mean boundary-layer characteristics for stable boundary-layer simulations over roughness length transitions. $\tau_{\mathrm{se},1}\tau_{\mathrm{se},2}^{-1}$ is the ratio of the equilibrium stress from the rougher patch over the equilibrium stress from the smoother patch

Case	L_{c} (m)	$z_{\mathrm{o},1}$ (m)	$z_{\mathrm{o},2}$ (m)	δ (m)	u_* (m s^{-1})	θ_* (K)	L (m)	$\tau_{\mathrm{se},1}\tau_{\mathrm{se},2}^{-1}$
A1	400	10^{-1}	10^{-2}	168	0.249	0.0398	105	1.84
A2	200	10^{-1}	10^{-2}	168	0.249	0.0398	104	1.89
A3	100	10^{-1}	10^{-2}	170	0.248	0.0396	104	1.98
B1	400	10^{-1}	10^{-3}	165	0.236	0.0379	98	2.95
B2	200	10^{-1}	10^{-3}	166	0.234	0.0378	98	3.19
B3	100	10^{-1}	10^{-3}	167	0.232	0.0374	97	3.60
C1	400	10^{-1}	10^{-4}	163	0.226	0.0365	94	4.39
C2	200	10^{-1}	10^{-4}	165	0.223	0.0362	93	4.96
C3	100	10^{-1}	10^{-4}	167	0.222	0.0358	92	5.89
D1	400	10^{-2}	10^{-3}	149	0.220	0.0370	88	1.60
D2	200	10^{-2}	10^{-3}	149	0.220	0.0369	88	1.65
D3	100	10^{-2}	10^{-3}	150	0.220	0.0369	88	1.81
E1	400	10^{-2}	10^{-4}	146	0.210	0.0355	83	2.39
E2	200	10^{-2}	10^{-4}	147	0.209	0.0354	83	2.55
E3	100	10^{-2}	10^{-4}	147	0.210	0.0354	83	2.97
F1	400	10^{-3}	10^{-4}	134	0.196	0.0342	75	1.48
F2	200	10^{-3}	10^{-4}	134	0.196	0.0342	75	1.54
F3	100	10^{-3}	10^{-4}	134	0.196	0.0342	75	1.65

3.2.1 Two-Dimensional Boundary-Layer Structure

The aerodynamic roughness length transitions have a direct impact on the surface shear stress and heat flux. Figure 3 shows the spanwise-averaged values of the surface shear-stress magnitude ($\tau_{\mathrm{s}}u_*^{-2}$) and heat flux ($H_{\mathrm{s}}u_*^{-1}\theta_*^{-1}$) for the C1–C3 cases plotted against the non-dimensional streamwise distance $x\delta^{-1}$. As expected, the rougher patches result in much larger spanwise-averaged surface shear-stress magnitude values relative to the smooth patches. The shear-stress magnitude reaches a maximum immediately after the smooth-to-rough transition and then rapidly decays to an equilibrium value over the rough patch. After the rough-to-smooth transition, τ_{s} exhibits a minimum value and then slowly increases with streamwise distance. The ratio between the equilibrium surface shear-stress values over the rough and smooth patches $\tau_{\mathrm{se},1}\tau_{\mathrm{se},2}^{-1}$ is tabulated in Table 2. In general, this ratio increases with increasing $z_{\mathrm{o},1}z_{\mathrm{o},2}^{-1}$ and with increasing patch size. It is interesting to note that all of these ratios are larger than the ratio between the surface shear stresses of the two homogeneous cases with the same aerodynamic roughness lengths as those used for the heterogeneous patch distribution (see Table 1).

The spanwise-averaged surface heat flux shows the exact same trends and nearly identical relative values as τ_{s} but with the opposite sign. This identical but inverse behaviour is a result of the chosen surface boundary condition, described in Sect. 2.1, that assumes $z_{\mathrm{o}} = z_{\mathrm{t}}$. As a result of this assumption the magnitude of the normalized surface heat flux is expected to track

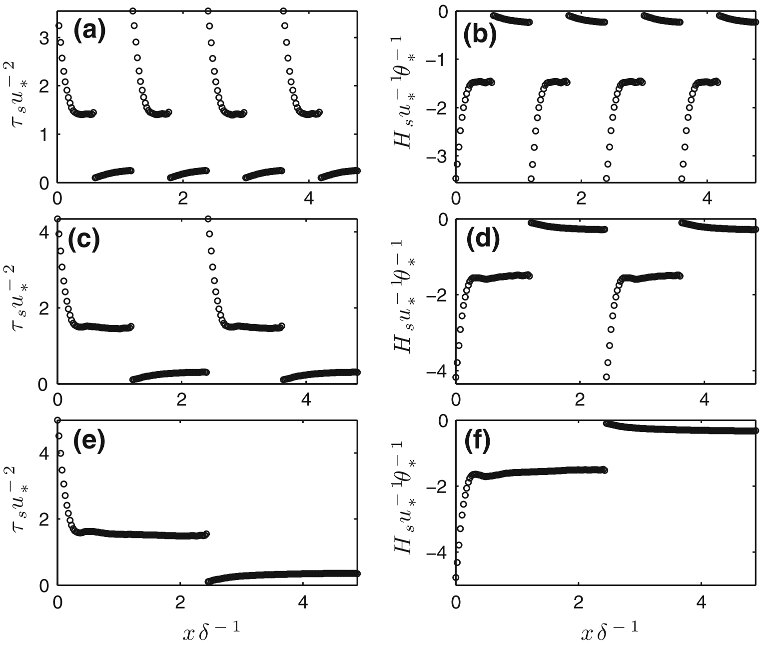

Fig. 3 Normalized surface-flux distributions averaged in the spanwise direction over streamwise transitions in aerodynamic roughness length: **a**, **b** are $\tau_{\mathrm{S}} u_*^{-2}$ and $H_{\mathrm{S}} u_*^{-1} \theta_*^{-1}$, respectively for case C3; **c**, **d** are the same for case C2; **e**, **f** are for case C1

that of the normalized surface shear-stress magnitude. Furthermore, because of the nature of the chosen boundary condition formulation (i.e., local application of Monin–Obukhov similarity theory), the primary mechanism driving the surface heat-flux distribution is the surface shear-stress distribution.

The surface-flux distributions are directly linked to the structure of the IBL that forms as a result of the rough-to-smooth and smooth-to-rough transitions. The IBL grows over each patch up to a height where the IBLs blend and the flow becomes homogeneous. Figure 4 illustrates the momentum IBL structure for simulations C1–C3 by plotting the spanwise-averaged non-dimensional velocity gradient deviation from the plane-averaged values ($\langle \Phi_{\mathrm{M}} \rangle_{\mathrm{t,y}} - \langle \Phi_{\mathrm{M}} \rangle_{\mathrm{t,x,y}}$ where $\langle\ \rangle_{\mathrm{t,y}}$ indicates averaging in time and in the spanwise direction, and $\langle\ \rangle_{\mathrm{t,x,y}}$ indicates averaging in time and over a plane). This is shown as a function of the non-dimensional height in the lowest part of the domain. The black lines indicate the locations in the flow where the deviation $= 0$ and the local velocity profiles have an inflection. Near the surface, this is also where the non-dimensional gradient is in equilibrium with the local surface fluxes at that streamwise location. Over individual patches the near-surface flow is not in equilibrium with the local surface fluxes as a result of the advection of higher momentum fluid to a lower momentum location after a smooth-to-rough transition, and lower momentum fluid to a higher momentum location after a rough-to-smooth transition.

The black equilibrium lines in Fig. 4 indicate the IBL height (Bou-Zeid et al. 2004). The IBL height grows with downstream distance from a transition as the impact of the surface diffuses upward. The IBL height grows at the same rate with downstream distance for both rough-to-smooth and smooth-to-rough transitions. Multiple previous studies have found this same result for IBLs in the neutral ABL (Glendening and Lin 2002; Bou-Zeid et al. 2004; Stoll

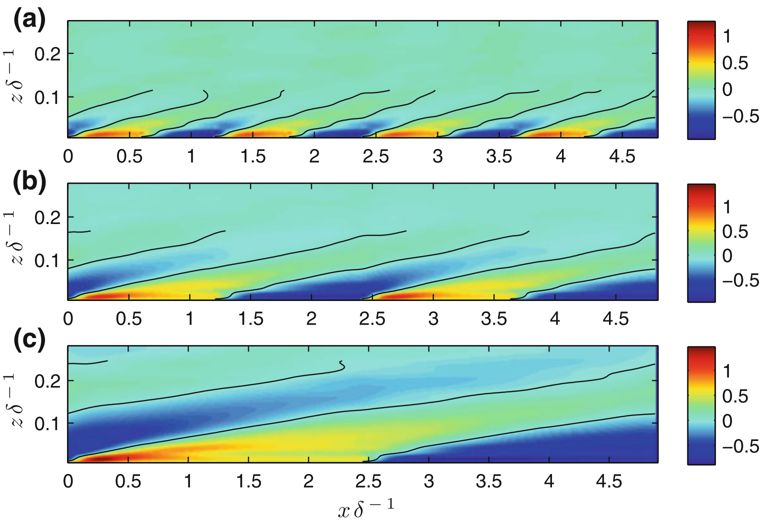

Fig. 4 Deviation of the spanwise-averaged value of the non-dimensional velocity gradient from the plane-averaged value ($\langle \Phi_M \rangle_{t,y} - \langle \Phi_M \rangle_{t,x,y}$) for cases C3 (**a**), C2 (**b**), and C1 (**c**) with IBLs highlighted in *black*. Only the lowest 45 m of the domain are shown

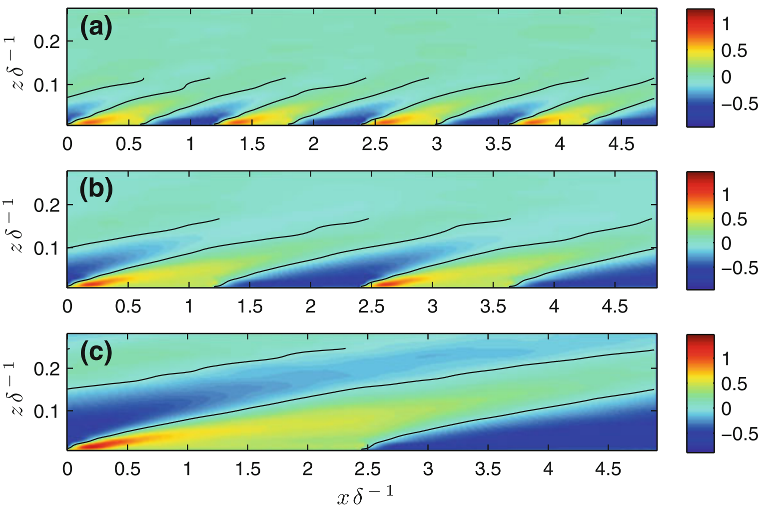

Fig. 5 Deviation of the spanwise-averaged value of the non-dimensional temperature gradient from the plane-averaged value ($\langle \Phi_H \rangle_{t,y} - \langle \Phi_H \rangle_{t,x,y}$) for cases C3 (**a**), C2 (**b**), and C1 (**c**) with IBLs highlighted in *black*. Only the lowest 45 m of the domain are shown

and Porté-Agel 2006a). Also apparent from Fig. 4 is that the growth rate of the momentum IBL height increases as the patch size decreases. This behaviour is characteristic of all of the heterogeneous test cases.

The thermal IBL behaves in a similar manner to the momentum IBL. Figure 5 shows the spanwise-averaged non-dimensional temperature gradient deviation from the plane-averaged values for the three cases in group C, in the lowest part of the domain. The IBL height for heat is indicated by the black equilibrium lines. Similarly to momentum, the thermal IBL height

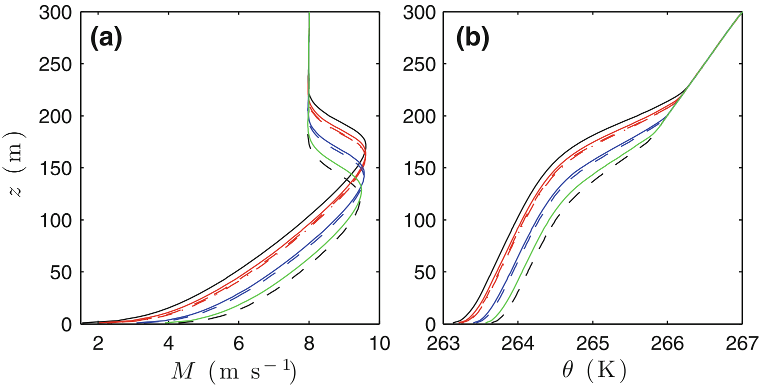

Fig. 6 Mean profiles of wind speed (**a**) and potential temperature (**b**) from SBL simulations over step changes in aerodynamic roughness length. *Linestyle* (*red solid line*) is for simulation A2, (*red dashed line*) is for simulation B2, (*red dashed-dotted line*) is for simulation C2, (*blue solid line*) is for simulation D2, (*blue dashed line*) is for simulation E2, and linestyle (*green solid line*) is for simulation F2. Two homogeneous simulations are shown for comparison using linestyles defined in Table 1

grows at the same rate with downstream distance from a transition regardless of whether the transition is rough-to-smooth or smooth-to-rough. Over individual patches, the non-dimensional temperature gradient is not in equilibrium with the local fluxes due to advection from upstream locations with different temperatures. Also apparent when comparing the IBLs of momentum and heat for the same case, is that the thermal IBL grows at a faster rate than does the momentum IBL height.

3.2.2 Vertical Profiles

Figure 6 displays the mean wind-speed and potential temperature profiles from a selection of the heterogeneous simulations. Two of the homogeneous cases from Sect. 3.1 are also shown in the plots for comparison. The heterogeneous cases all reproduce the main features of a continuously turbulent SBL: the existence of a nocturnal jet just below the boundary-layer height in the wind-speed profiles and positive curvature throughout the boundary layer for the potential temperature profiles (Nieuwstadt 1985). One of the most striking conclusions that can be drawn from both plots is that the aerodynamic roughness length heterogeneity has minimal impact on the shape of the mean profiles and only tends to shift them. Also, the profiles of all of the heterogeneous simulations of identical $z_{o,1}$ values, regardless of the $z_{o,2}$ value or the patch size, nominally, collapse (including those not pictured). These collapsed profiles always lie between the mean profiles of the homogeneous cases with the same z_o values as those used in the heterogeneous case. More specifically, they tend to lie closer to the profiles of the homogeneous cases of z_o values equal to the rougher of the two values used in the heterogeneous cases. This holds for both the wind speed (Fig. 6a) and potential temperature (Fig. 6b). Even simulations C1–C3, in which the surface has a $z_{o,2}$ value of only 10^{-4} m, create profiles close to the $z_o = 10^{-1}$ m homogeneous case. This suggests that the rougher of the two surfaces has a larger impact on controlling the mean flow than does the smoother surface. Wood (1982) came to this same conclusion based on wind-tunnel data. These trends are also seen in the bulk boundary-layer parameters in Table 2 where all of the values for the heterogeneous cases lie between those of the two homogeneous cases with

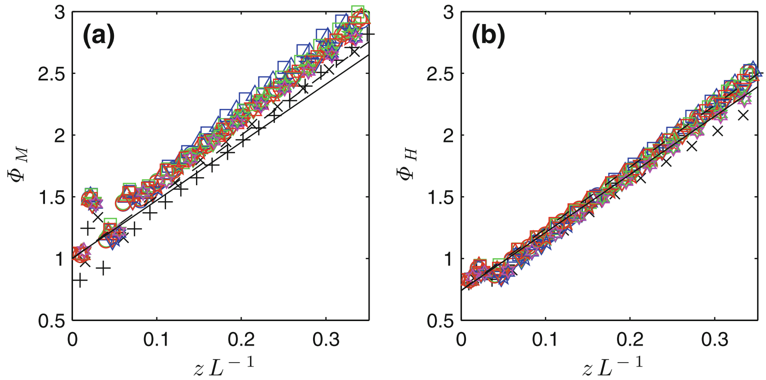

Fig. 7 Non-dimensional velocity gradient (**a**) and potential temperature gradient (**b**) as functions of zL^{-1} in the lowest 40 m of the domain. The formulations given as Eqs. 12 and 13 are shown as the *lines* in the two plots respectively. The *solid lines* use $\gamma_m = \gamma_h = 4.7$. The *dashed lines* use $\gamma_m = \gamma_h = 5.0$. The (*open circle*), (*open triangle*), (*open square*), (*inverted open triangle*), (*open star*), and (*six pointed open star*) *symbols* are for simulation groups A, B, C, D, E, and F, respectively. *Red*, *green*, and *blue symbols* are for 400, 200, and 100 m patch length scale cases, respectively. Two homogeneous simulations are shown for comparison using *symbols* defined in Table 1

the same two z_o values used in the heterogenous aerodynamic roughness length distribution. The values are also typically closer to the values of the rougher homogeneous case.

The subject of this research is surface-layer modelling. Most surface-flux models rely, in one form or another, on Monin–Obukhov similarity theory (Delage 1997; Brutsaert 1998). To look at the surface layer in greater detail and explore the validity of Monin–Obukhov similarity theory over heterogeneous aerodynamic roughness length distributions, the non-dimensional shear and potential temperature from the lowest 40 m of the domain are plotted as functions of zL^{-1} in Fig. 7 for all of the heterogeneous cases. The non-dimensional gradients from the LES are compared with the relationships of Businger et al. (1971) (Eqs. 12 and 13) with γ_m and γ_h equal to both 4.7 and 5.0. Two of the homogeneous cases from Sect. 3.1 are also included for comparison. The heterogeneous simulations' non-dimensional gradients have a high level of agreement with the similarity relationships and are nearly indistinguishable from the homogeneous cases presented in Fig. 2. Bou-Zeid et al. (2004) found this same result for flow over heterogeneous aerodynamic roughness length patches in the neutral ABL. In contrast, Stoll and Porté-Agel (2009) did not find this to be the case for flow over heterogeneous surface temperature patches in the SBL. Because the heterogeneous z_o has not changed the functional relationship between the mean wind speed and potential temperature and the surface-layer stability parameter, Monin–Obukhov similarity theory should still be valid to calculate the mean fluxes for the heterogeneous z_o configurations used here.

4 Evaluation of Heterogeneous Surface-Flux Models for z_o Transitions

In this section, the LES velocity and potential temperature fields are used to evaluate the ability of the surface-flux models discussed in Sect. 1.1 to properly account for heterogeneous z_o distributions. Examination of the heterogeneous simulation mean profiles and non-dimensional gradients in Sect. 3.2 showed that the surface property distributions used in this study do not functionally change the relationship between the grid-average surface fluxes and the grid-averaged wind speed and potential temperature. This is promising for the application of Monin–Obukhov similarity, but it does not address the issue of how to specify the roughness lengths at the grid scale of a large-scale model. A common way to accomplish this is through the specification of $z_{o,e}$ and $z_{t,e}$. The LES wind-speed and potential temperature profiles (Fig. 6) in combination with average surface heat flux and shear stress (Table 2) can be used to calculate the $z_{o,e}$ and $z_{t,e}$ for each case.

4.1 Effective Aerodynamic Roughness Length from LES

Two independent methods are used to evaluate the effective aerodynamic roughness length from the simulations. The first uses a least-squares fit to a log-linear wind-speed profile to calculate $z_{o,e}$, following Bou-Zeid et al. (2004). It gives $z_{o,e}$ values that are consistent with Taylor's (1987) definition of $z_{o,e}$ as the value that best agrees with the mean velocity profile over a heterogeneous surface.

The second method used to calculate $z_{o,e}$ is based on the definition of Mason (1988). Instead of finding the $z_{o,e}$ that best matches the average wind speed, the method calculates the value of $z_{o,e}$ that gives the best agreement with the average surface stress. This is accomplished by replacing the left-hand side of Eq. 1 with $\sum_{\mathrm{i}} f_{\mathrm{i}} \langle \tau_{\mathrm{s}} \rangle_{\mathrm{i}}$. The patch-averaged surface-stress values are directly evaluated from the local LES surface-stress values and $z_{o,e}$ is then calculated using a least-squares fit to the LES average wind-speed profile.

The $z_{o,e}$ values determined by these two methods are different (Mason 1988; Schmid and Bünzli 1995), and those determined through the stress method are always larger than those determined from the velocity method. Values determined from both methods are listed in Table 3. All values are calculated using data between heights of 5 and 40 m and assuming that the stability correction for momentum of Businger et al. (1971) describes the results accurately. Note that this stability correction is derived from the integration of Eq. 12, which showed acceptable agreement with all the heterogeneous cases. Still, the assumption of a form of the stability corrections will introduce some error in the $z_{o,e}$ calculations. The effective aerodynamic roughness length values show a dependance on the ratio of $z_{o,1}$ to $z_{o,2}$, on $z_{o,1}$ itself, and on L_{c}.

4.2 Effective Roughness Length for Heat from LES

Researchers typically argue that the effective roughness length for heat ($z_{t,e}$) should be determined as a function of $z_{o,e}$ (e.g., Claussen 1991; Arola 1999). The relationship between $z_{o,e}$ and $z_{t,e}$ can be calculated from the LES data. In homogeneous flows over roughness comprised of randomly distributed elements, the inverse Stanton number (B^{-1}) defines the relationship between z_o and z_t (Owen and Thomson 1963; Garratt 1992). For flow over heterogeneous roughness patches an equivalent relationship can be defined for $z_{o,e}$ and $z_{t,e}$ where $B^{-1} = \ln(z_{o,e} z_{t,e}^{-1})\kappa^{-1}$. Using the LES data, B^{-1} was calculated following the general methodology described in Beljaars and Holtslag (1991) using $B^{-1} = (\theta_o - \theta_s)\theta_*^{-1}$, where θ_o is the temperature at $z = z_{o,e}$. θ_o was calculated from each simulation by extrapolating down from the lowest computational level using the log-linear profile. The $z_{o,e}$ values determined using the stress method were used here in order to maintain consistency with the IBL models given in Sect. 1.1. The B^{-1} values are shown in Table 3 and range from 5.0 to 8.2, with a mean value of ≈ 6.8. This range of values is in agreement with many previous studies (e.g., Chamberlain 1966; Thom 1972; Garratt and Hicks 1973; Beljaars and Holtslag 1991), but unlike those studies the values found here are not for a homogeneous surface with random roughness elements. Instead, the difference between $z_{o,e}$ and $z_{t,e}$ can be directly attributed to the effect

Table 3 LES-determined surface-layer parameters including: effective aerodynamic roughness lengths ($z_{o,e}$) determined using the velocity and stress methods ($z_{o,e,V}$ & $z_{o,e,S}$, respectively), B^{-1} values, and blending heights for momentum (h_b) and heat ($h_{b,h}$)

Case	$z_{o,e,V}$ (m)	$z_{o,e,S}$ (m)	B^{-1}	h_b (m)	$h_{b,h}$ (m)
A1	2.62×10^{-2}	2.98×10^{-2}	5.0	39.2	25.7
A2	2.66×10^{-2}	3.15×10^{-2}	5.1	24.1	16.7
A3	2.78×10^{-2}	3.53×10^{-2}	5.9	16.1	12.1
B1	1.30×10^{-2}	1.99×10^{-2}	5.8	38.0	24.6
B2	1.40×10^{-2}	2.37×10^{-2}	6.2	23.1	16.4
B3	1.57×10^{-2}	3.04×10^{-2}	6.1	16.1	11.9
C1	8.00×10^{-3}	1.69×10^{-2}	7.0	38.0	23.9
C2	8.70×10^{-3}	2.12×10^{-2}	6.9	22.9	16.2
C3	1.07×10^{-2}	3.00×10^{-2}	7.4	16.1	12.0
D1	2.65×10^{-3}	2.96×10^{-3}	6.4	30.8	20.4
D2	2.71×10^{-3}	3.12×10^{-3}	6.7	19.7	13.7
D3	2.84×10^{-3}	3.38×10^{-3}	6.8	13.9	9.8
E1	1.27×10^{-3}	1.83×10^{-3}	7.5	29.6	19.5
E2	1.33×10^{-3}	2.07×10^{-3}	7.6	19.2	13.3
E3	1.51×10^{-3}	2.53×10^{-3}	7.7	14.2	9.6
F1	2.64×10^{-4}	2.89×10^{-4}	8.1	24.5	16.5
F2	2.63×10^{-4}	2.94×10^{-4}	8.1	16.8	12.9
F3	2.72×10^{-4}	3.07×10^{-4}	8.2	13.8	7.5

of the heterogeneous roughness length distribution. The LES surface boundary conditions apply Monin–Obukhov similarity theory locally, and at every surface grid point specify that $z_o = z_t$ (see Sect 2.1). Because $z_o = z_t$ locally, any differences between $z_{o,e}$ and $z_{t,e}$ can be attributed to surface heterogeneity. Most effective aerodynamic roughness length models do not have the ability to account for the effect of patch scale heterogeneity on B^{-1} and instead use ad hoc values determined for homogeneous surfaces. The exception to this is WM91.

4.3 Blending Heights from LES

Many $z_{o,e}$ and $z_{t,e}$ parametrizations use the blending heights for momentum and heat (h_b and $h_{b,h}$) as internal parameters (e.g., Wood and Mason 1991; Claussen 1991; Bou-Zeid et al. 2004). Here, h_b and $h_{b,h}$ were identified in the LES results using the difference between the spanwise-averaged and plane-averaged values of wind speed and temperature: $\langle u\rangle_{t,y} - \langle u\rangle_{t,x,y}$ and $\langle \theta\rangle_{t,y} - \langle \theta\rangle_{t,x,y}$, respectively. The height of the first significant minimum in the difference between the upper and lower quartiles of these quantities was chosen as the blending height for each, following Bou-Zeid et al. (2004). The blending heights based on wind speed were found to be higher than the blending heights based on potential temperature by an average of 1.5 times. Schmid and Bünzli (1995) suggested that the blending height should be identified as the height at which the vertical fluxes of momentum and heat become essentially homogeneous. This definition was also tested, by identifying the heights at which the first minimum difference was found between the quartiles of the differences of the spanwise-

Table 4 Effective aerodynamic roughness lengths ($z_{o,e}$) determined using the models of Taylor (1987) (Eq. 3), and Mason (1988) (Eq. 4), as well as BZ04 (Eq. 6), all paired with Eq. 7. Also given are $z_{o,e}$ and B^{-1} values from WM91 (Eq. 4 with stability correction). The LES $z_{o,e}$ values derived using the stress method ($z_{o,e,S}$) are repeated here for comparison

Case	$z_{o,e,S}$ (m)	Taylor	Mason	BZ04	WM91	
		$z_{o,e}$ (m)	$z_{o,e}$ (m)	$z_{o,e}$ (m)	$z_{o,e}$ (m)	B^{-1}
A1	2.98×10^{-2}	3.16×10^{-2}	4.60×10^{-2}	4.14×10^{-2}	4.30×10^{-2}	4.2
A2	3.15×10^{-2}	3.16×10^{-2}	4.76×10^{-2}	4.24×10^{-2}	4.56×10^{-2}	3.8
A3	3.53×10^{-2}	3.16×10^{-2}	4.95×10^{-2}	4.35×10^{-2}	4.81×10^{-2}	3.3
B1	1.99×10^{-2}	1.00×10^{-2}	3.27×10^{-2}	2.49×10^{-2}	3.10×10^{-2}	4.4
B2	2.37×10^{-2}	1.00×10^{-2}	3.55×10^{-2}	2.65×10^{-2}	3.42×10^{-2}	3.9
B3	3.04×10^{-2}	1.00×10^{-2}	3.87×10^{-2}	2.84×10^{-2}	3.78×10^{-2}	3.5
C1	1.69×10^{-2}	3.16×10^{-3}	2.77×10^{-2}	1.83×10^{-2}	2.64×10^{-2}	4.5
C2	2.12×10^{-2}	3.16×10^{-3}	3.10×10^{-2}	2.03×10^{-2}	3.01×10^{-2}	4.0
C3	3.00×10^{-2}	3.16×10^{-3}	3.48×10^{-2}	2.25×10^{-2}	3.41×10^{-2}	3.5
D1	2.96×10^{-3}	3.16×10^{-3}	4.21×10^{-3}	3.91×10^{-3}	4.01×10^{-3}	5.7
D2	3.12×10^{-3}	3.16×10^{-3}	4.30×10^{-3}	3.97×10^{-3}	4.17×10^{-3}	5.3
D3	3.38×10^{-3}	3.16×10^{-3}	4.42×10^{-3}	4.04×10^{-3}	4.33×10^{-3}	4.9
E1	1.83×10^{-3}	1.00×10^{-3}	2.61×10^{-3}	2.11×10^{-3}	2.50×10^{-3}	6.1
E2	2.07×10^{-3}	1.00×10^{-3}	2.77×10^{-3}	2.20×10^{-3}	2.71×10^{-3}	5.5
E3	2.53×10^{-3}	1.00×10^{-3}	2.97×10^{-3}	2.32×10^{-3}	2.92×10^{-3}	5.2
F1	2.89×10^{-4}	3.16×10^{-4}	3.97×10^{-4}	3.76×10^{-4}	3.82×10^{-4}	7.3
F2	2.94×10^{-4}	3.16×10^{-4}	4.03×10^{-4}	3.80×10^{-4}	3.94×10^{-4}	6.7
F3	3.07×10^{-4}	3.16×10^{-4}	4.10×10^{-4}	3.85×10^{-4}	4.05×10^{-4}	6.0

and plane-averaged fluxes. Blending heights determined from the fluxes are expected to be larger than those determined from average primitive variables (Wood and Mason 1991; Garratt 1992). We found that estimates based on the momentum flux exceed those based on the wind speed by up to 60 % and estimates based on the heat flux exceed those based on the potential temperature by 80–180 %. Although the flux-based estimates are generally larger than estimates based on average variables, the trends in blending height values as functions of patch length and z_o transition magnitude are the same. Here, blending height estimates from average variables, presented in Table 3, are used for our analysis.

4.4 Model Application

Table 4 gives estimated $z_{o,e}$ values from the models discussed in Sect. 1.1. The range of B^{-1} values found using WM91 is also shown in Table 4 and the values are similar to those found from the LES data. The local flux values required for WM91 are determined using a tile model (Avissar and Pielke 1989). For BZ04, the values in Table 4 were found using their recommended value of $c_1 = 0.85$ in Eq. 6.

From the values in Table 3 we concluded that $z_{o,e}$ should depend on $z_{o,1}$, $z_{o,1}z_{o,2}^{-1}$, and L_c. The tested formulations, excluding the model of Taylor (1987), include this type of behaviour. Though the model of Taylor (1987) cannot produce a dependence on L_c, it does generate the best $z_{o,e}$ estimates for cases with minimal surface shear-stress variation. It is also apparent from Table 4 that Wood and Mason's (1991) additions to Mason's (1988) model improve estimates. Even though this method generates reasonable ratios for $z_{t,e}$ to $z_{o,e}$, the values of both are considerably larger than the LES equivalents. Of the models shown in Table 4, BZ04 does the best job of recreating the LES values but still consistently overestimates them. A likely source of this overestimation is the lack of any adjustment for atmospheric stability in the model. The justification for not including stability in the determination of $z_{o,e}$ is the idea that aerodynamic roughness length is a geometric function and should not change with stability (Bou-Zeid et al. 2007). While conceptually this idea has strong merit, it is questionable for the heterogeneous SBL for the following reasons. First, it is well accepted that vertical diffusion in the ABL, a central component of Eq. 6, is influenced significantly by stability (Mahrt 1998, 2000). Second, stability corrections in Monin–Obukhov theory are non-linearly related to the surface fluxes, and do not strictly commute with spatial averages. Therefore, it should be expected that the heterogeneous surface distribution of L should contribute non-linearly to surface fluxes. Lastly, from a practical standpoint the inclusion of stability corrections in Wood and Mason (1991) to Mason's (1988) model improves $z_{o,e}$ predictions and provides an estimate of B^{-1} avoiding the need to specify an ad hoc value.

Motivated by these ideas, and the fact that BZ04 produces data with the best agreement to the LES $z_{o,e}$ values, a modified version of their model is developed that incorporates stability corrections following the general methodology of WM91. This is accomplished by starting with the same scaling arguments previously verified in Garratt (1990) and used in BZ04. The argument is that the IBL height (h_{IBL}) grows as $\mathrm{d}h_{\mathrm{IBL}}\mathrm{d}x^{-1} \sim w_{\mathrm{rms}}\langle u(h_{\mathrm{IBL}})\rangle^{-1}$ and that $w_{\mathrm{rms}} = c_1 u_*$ in the near-surface region, where c_1 is the $O(1)$ constant discussed in Sect. 1.1. Unlike the derivation of BZ04, here the Businger et al. (1971) stability corrections are included when $u_*\langle u(h_{\mathrm{IBL}})\rangle^{-1}$ is replaced by a log-linear approximation. Upon integration of the result the new model is

$$h_{\mathrm{b}}\left[\ln\left(\frac{h_{\mathrm{b}}}{z_{\mathrm{o,e}}}\right)-1\right]+\frac{\beta_{\mathrm{m}}h_{\mathrm{b}}^2}{2L_{\mathrm{e}}}=c_1\kappa X_1, \tag{14}$$

where X_1 is the downstream distance at which the height of the IBL reaches the blending height. From examination of Fig. 4, it is seen that the momentum IBL appears to reach its blending height at a downstream distance, $X_1 \lesssim 2L_{\mathrm{c}}$. This is generally the case for all the simulations. Bou-Zeid et al. (2004) came to a similar conclusion in their neutral simulations. Like WM91, discussed in Sect. 1.1, Eq. 14 is combined with Eq. 8 to solve for $z_{\mathrm{o,e}}$ and h_{b}.

An equivalent model to Eq. 14 is also developed for $z_{\mathrm{t,e}}$ and $h_{\mathrm{b,h}}$. This is done following the same scaling arguments used for momentum, but instead assuming that $\mathrm{d}h_{\mathrm{IBL,h}}\mathrm{d}x^{-1} \sim \theta_{\mathrm{rms}}\langle\Delta\theta(h_{\mathrm{IBL}})\rangle^{-1}$ and that the root-mean-square of the temperature $\theta_{\mathrm{rms}} = c_2\theta_*$ in the near-surface region. After substitution of the log-linear temperature approximation for $\theta_*\langle\Delta\theta(h_{\mathrm{IBL}})\rangle^{-1}$ and integration of the result, the equation for $h_{\mathrm{b,h}}$ is

$$h_{\mathrm{b,h}}\left[\ln\left(\frac{h_{\mathrm{b,h}}}{z_{\mathrm{t,e}}}\right)-1\right]+\frac{\beta_{\mathrm{h}}h_{\mathrm{b,h}}^2}{2L_{\mathrm{e}}}=c_2\kappa X_2, \tag{15}$$

where c_2 is an $O(1)$ scaling constant and X_2 is the downstream distance at which the height of the thermal IBL reaches $h_{\mathrm{b,h}}$. The second assumption that $\theta_{\mathrm{rms}} = c_2\theta_*$ was tested using the simulation results. It was found that $\theta_{\mathrm{rms}}\theta_*^{-1}$ has a nearly constant value of ≈ 1.9 in the near-surface region across all the cases. Recall that c_1 contains, in part, the ratio of w_{rms} to u_* that has been shown to also be nearly constant throughout the near-surface region, and has a mean of ≈ 1.0 (Bou-Zeid et al. 2004). Thus, the simulation results indicate that c_2 should be nearly twice the value of c_1. This difference is also confirmed upon observation of the thermal IBL shown in Fig. 5 when compared to the momentum IBL shown in Fig. 4. The thermal IBL tends to grow at a faster rate than does the momentum IBL suggesting that a larger constant is needed to represent the slope. In addition, because $h_{b,h}$ is generally $< h_b$ (see Table 3), the downstream distance at which the thermal IBL is blended out is significantly less than the value of $\approx 2L_c$ found for momentum. Examination of the thermal IBL and blending height values leads to the conclusion that $X_2 \approx 1L_c$. Interestingly these values suggest that the combination of the coefficients on the right-hand side of Eqs. 14 and 15 should be approximately equal (i.e. $c_1(2L_c) \approx c_2(1L_c)$).

The complete version of the new model therefore consists of four equations that include the benefits of both BZ04 and WM91 models. The new model solves for $z_{o,e}$ and $z_{t,e}$ by combining Eq. 14 with Eq. 8 as well as Eq. 15 with Eq. 9 using the general iterative procedure outlined in Wood and Mason (1991). Local flux values required in the model are determined using a tile approach (Avissar and Pielke 1989).

Further exploration was done to determine the appropriate value for c_1 in BZ04 and for c_1 and c_2 in Eqs. 14 and 15 for the case of a heterogeneous SBL. As c_1 is increased, the IBL growth rate determined by the models also increases. Because the IBL grows at a different rate for each simulation, an optimum c_1 value for both IBL models was determined for each case using a least-squares fit to the LES data. This was done using the $z_{o,e,S}$ values given in Table 3 and by then applying the models at heights above the lowest computational level to avoid any bias that would be created by the boundary condition. For BZ04, the optimum c_1 values have a mean of ≈ 0.97 and a range between 0.72 and 1.29 with variability based primarily on L_c. The new model typically predicts a shallower IBL with more curvature than does BZ04 when using the same value of c_1. This results in the new model having a slightly larger value of ≈ 1.04 for the average optimum c_1 with a range from 0.76 to 1.36. The general trend and impact on the predicted thermal IBL heights by varying c_2 in Eq. 15 is similar to that explained for c_1. The same technique used to determine optimum values for c_1 was applied to find optimum values for c_2. These values were found to vary between 1.25 and 2.51 with a mean of ≈ 1.74. This finding supports the arguments made above that c_2 should be nearly twice the value of c_1.

Along with the $z_{o,e}$ values, blending heights were calculated using each of the models. Those found from the model of Mason (1988) and from WM91 (not shown) are much lower than those calculated from the simulations. In contrast, the blending heights calculated using BZ04 and the new model are in much closer agreement with the LES blending height values. When the optimum values for c_1 and c_2 are used in the new model, the accuracy of the blending heights versus those determined from the simulations is improved. This is most pronounced for blending heights < 20 m, which are improved up to 25 %. The improvement does not significantly change the values of $z_{o,e}$ when compared to using a single value for the constants for all of the cases. This negligible change in $z_{o,e}$ values is attributed to the fact that relatively large changes in h_b correspond to only minor changes to $z_{o,e}$ (Bou-Zeid et al. 2004). For this reason, it was decided that using constant values for c_1 and c_2 would be satisfactory for the range of heterogeneous z_o distributions used here. In addition, as discussed above X_1 and X_2 are constant factors of L_c that can be combined with c_1 and c_2. Using the mean optimum values of c_1 and c_2 this results in $c_1 X_1 \approx 2.08 L_c$ and $c_2 X_2 \approx 1.74 L_c$. Motivated by the lack of a strong dependence of model estimates for $z_{o,e}$ and $z_{t,e}$ on the values of c_1 and c_2 and by the similarity of $c_1 X_1$ and $c_2 X_2$, sensitivity tests were carried out to determine whether a single constant could be used for $c_1 X_1$ and $c_2 X_2$. These tests concluded that using $c_1 X_1 = c_2 X_2 = 1.85 L_c$ produces the smallest net difference between the modelled surface fluxes and the LES results (surface-flux estimates are elaborated on below). Hereafter this value is used when evaluating Eqs. 14 and 15.

Fig. 8 Model blending height for momentum versus blending heights determined from quartiles of wind speed from the LES data. For BZ04, $c_1 = 0.85$. For the new model given by Eqs. 14, 15, 8, and 9, $c_1 X_1 = c_2 X_2 = 1.85 L_c$. *Red symbols* are from BZ04 while *blue symbols* are from the modified model. The (*open circle*), (*open triangle*), (*open square*), (*inverted open triangle*), (*open star*), and (*open star of David*) *symbols* are for simulation groups A, B, C, D, E, and F, respectively

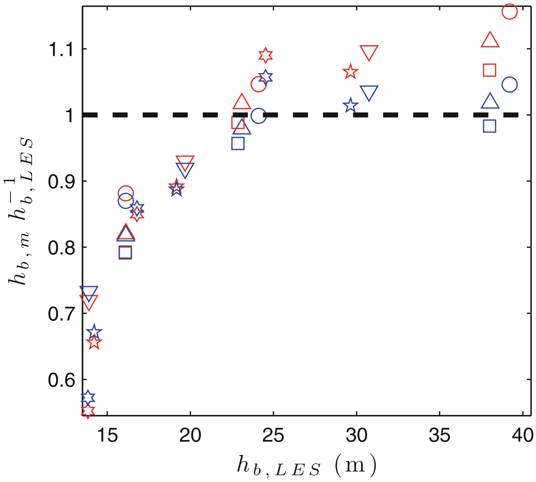

The model blending heights ($h_{\mathrm{b,m}}$) determined from the new model and from BZ04 are compared to the LES values ($h_{\mathrm{b,LES}}$) in Fig. 8. The new model produces more accurate h_{b} values for 11 of the 18 simulations. The remaining seven cases have $< 4\,\%$ difference between their h_{b} values. Each of the models has difficulty recreating the LES-determined blending height values for blending heights < 20 m because each specifies $c_1 X_1$ as a constant multiple of L_{c} for all cases. As mentioned previously, this has little impact on the calculated $z_{\mathrm{o,e}}$ values. The new model also calculates $h_{\mathrm{b,h}}$ and, as with WM91, finds $h_{\mathrm{b,h}} \approx h_{\mathrm{b}}$ for each case. This is inconsistent with the LES blending height values from Table 3 and overpredicts the LES values of $h_{\mathrm{b,h}}$ by $\approx 50\,\%$.

The effective aerodynamic roughness lengths determined using the modified and original versions of BZ04 ($z_{\mathrm{o,e,m}}$) are compared with the LES equivalents ($z_{\mathrm{o,e,LES}}$) in Fig. 9. The new model generally predicts lower values than BZ04 and improves the accuracy of 10 of the 18 $z_{\mathrm{o,e}}$ estimates. It also does a better job at matching the rate at which $z_{\mathrm{o,e}}$ changes as a function of L_{c}. This is a result of the stability correction accounting for the change in

Fig. 9 $z_{\mathrm{o,e}}$ values determined from the models plotted against the LES $z_{\mathrm{o,e}}$ values determined using the stress method. *Red symbols* are from BZ04 while *blue symbols* are from the new model given by Eqs. 14, 15, 8, and 9. The (*open circle*), (*open triangle*), (*open square*), (*inverted open triangle*), (*open star*), and (*open star of David*) *symbols* are for simulation groups A, B, C, D, E, and F, respectively

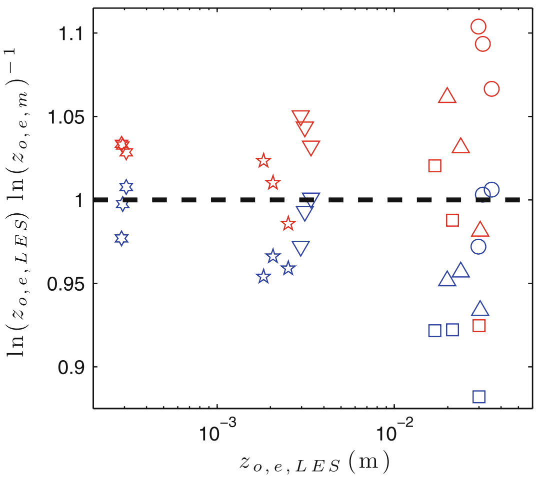

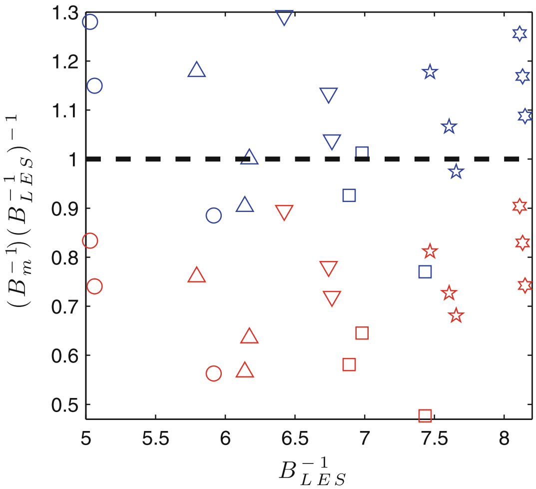

Fig. 10 B^{-1} values determined from the models plotted against the LES values presented in Table 3. *Red symbols* are from WM91 while *blue symbols* are from the new model given by Eqs. 14, 15, 8, and 9. The (*open circle*), (*open triangle*), (*open square*), (*inverted open triangle*), (*open star*), and (*open star of David*) *symbols* are for simulation groups A, B, C, D, E, and F, respectively

stratification within a single group of simulations (e.g., group C). Examination of Tables 2 and 4 reveals, that as the patch size decreases, there is an increase in bulk stability as well as a sharp increase in $z_{o,e}$. BZ04 does calculate larger $z_{o,e}$ values for smaller patch sizes but the changes are not as significant as indicated in the LES results. Because of this, as patch length decreases, the ratio of $z_{o,e}$ values calculated using BZ04 to those determined from the LES also significantly decreases. The inclusion of the stability corrections in the new model, given by Eqs. 14 and 15, accounts for this stability-to-L_c relation. This manifests itself as the elimination of the steep negative slope observed in each group in the BZ04 model estimates (red symbols with the same marker in Fig. 9) by the new model (blue symbols with the same marker in Fig. 9).

The new model also solves for $z_{t,e}$. When combined with the $z_{o,e}$ values, model estimates for B^{-1} can be calculated. These B^{-1} values are shown in Fig. 10 along with the B^{-1} values determined using WM91 (B_m^{-1}). Both models are compared to the LES values from Table 3 (B_{LES}^{-1}). The new model produces B^{-1} values that range from a minimum value of 5.2 to a maximum of 10.2. In general, these values have better agreement with the LES-based estimates than do the values from WM91 (see Table 4), which tends to underestimate the LES values. Specifically, in 15 of the 18 cases the new model outperforms WM91.

More important than the accuracy of the individual h_b, $z_{o,e}$, and B^{-1} values is the ability of those values, when used in Eqs. 1 and 2, to model the LES average fluxes. Surface-stress and heat-flux values calculated from the bulk model ($\tau_{s,m}$ and $H_{s,m}$ from Eqs. 1 and 2, respectively), using the effective aerodynamic roughness length values from BZ04 and the new model, are presented in Fig. 11. The model estimates are normalized by the LES-surface flux values ($\tau_{s,LES}$ and $H_{s,LES}$) and plotted for the large-scale model lowest computational level heights (Z_m) ranging from 10 to 55 m. The bulk method uses a direct integration of Eqs. 12 and 13. Because these equations were used in the calculation of the LES $z_{o,e}$ values, the model surface-flux estimates are expected to be close to the average LES surface fluxes so long as $z_{o,e,m} \approx z_{o,e,LES}$ and $B_m^{-1} \approx B_{LES}^{-1}$. The BZ04 results shown in Fig. 11 use a constant value of $B^{-1} = 6$, found to produce the most accurate results with this model. Larger or smaller B^{-1} values degrade the performance of BZ04. If $z_{t,e}$ is allowed to simply equal the $z_{o,e}$ values from BZ04 (i.e. $B^{-1} = 0$), as might be suggested by the LES boundary

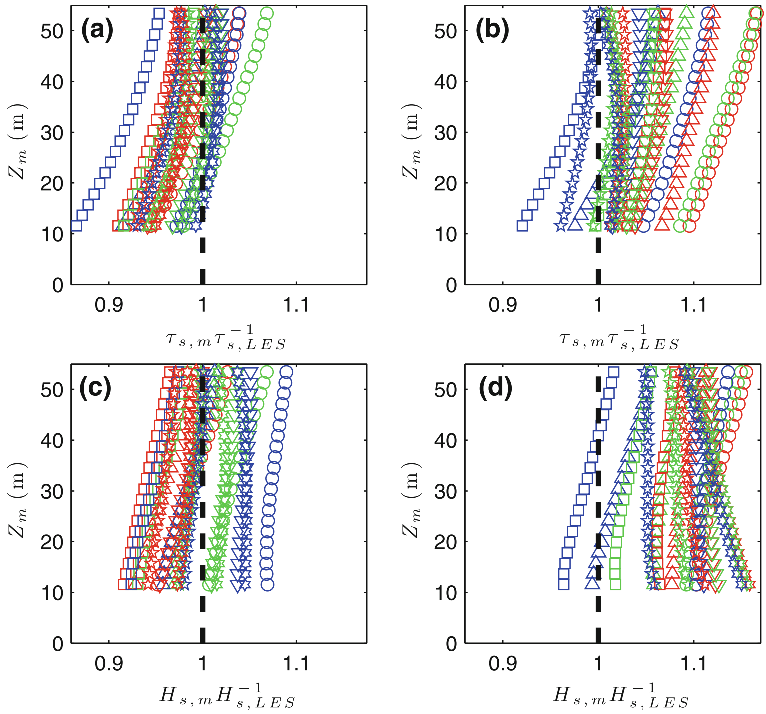

Fig. 11 Modelled surface shear stress [(**a**) and (**b**)] and surface heat flux [(**c**) and (**d**)] divided by the average LES equivalents. Modelled values are computed from the bulk similarity method using the effective aerodynamic roughness length estimates from the new model [(**a**) and (**c**)] and using the $z_{o,e}$ values from BZ04 combine with $B^{-1} = 6$ [(**b**) and (**d**)]. Z_m is the height of the lowest computational level in a large-scale atmospheric model. The (*open circle*), (*open triangle*), (*open square*), (*inverted open triangle*), (*open star*), and (*open star of David*) *symbols* are for simulation groups A, B, C, D, E, and F, respectively. *Red*, *green*, and *blue symbols* are for 400, 200, and 100 m patch length scale cases, respectively

condition, the bulk model produces surface shear-stress results comparable to those in Fig. 11, but considerably overestimates the surface heat flux.

The effective aerodynamic roughness length values calculated by both models do a good job of recreating the LES fluxes as shown in Fig. 11. The new model produces better results when all the cases are considered collectively, and generally predicts lower values than BZ04. The fluxes from the new model tend to cluster together more closely, and do so closer to the LES values than do the fluxes from BZ04. This is likely a result of the fact that the new model produces a value for B^{-1} for each individual case providing a mechanism to represent the impact of heterogeneity on $\langle H_s \rangle$. The new model also has a weaker dependence on Z_m. The heat fluxes shown in Fig. 11c illustrates this strongly. The predictions from the new model are much closer to constant with Z_m than are those in Fig. 11d. In Fig. 11d, the positive and negative slopes seen for some of the cases are caused by the value chosen for B^{-1} being higher and lower, respectively, than what is determined from the LES data.

5 Summary

Large-eddy simulations, based on GABLS1, were used to examine the effects of aerodynamic roughness length transitions on mean profiles of wind speed and potential temperature and the surface fluxes of heat and momentum in the stable boundary layer. Six different z_o combinations were considered: 0.1–0.01, 0.1–0.001, 0.1–0.0001, 0.01–0.001, 0.01–0.0001, and 0.001–0.0001 m. Each combination was tested with three different patch sizes of 100, 200, and 400 m. These patch sizes range from roughly one-half to roughly twice the mean boundary-layer height from a simulation with a homogeneous $z_o = 0.1$ m. For the range of aerodynamic roughness length combinations and patch lengths studied here, the heterogeneity was found to have very little effect on the functional relationship between the mean wind speed and potential temperature and the surface-layer stability parameter. Although the average values are not functionally affected, locally the z_o distributions have a strong impact on the velocity and temperature fields. In the near-surface region the flow is generally not in equilibrium with the local surface with a distinct IBL forming after each transition. The growth rate of each IBL is indistinguishable for rough-to-smooth or smooth-to-rough transitions, and the thermal IBL grows at a faster rate than the momentum IBL.

Five effective aerodynamic roughness length formulations were also tested. One of those was a new formulation developed here that takes advantage of the benefits of the models presented in Wood and Mason (1991) and Bou-Zeid et al. (2004). This new model accounts for the effects of atmospheric stability while solving for the effective roughness lengths for both momentum and heat. Of the tested formulations, only the formulation of Taylor (1987) failed to match the trends from LES-derived $z_{o,e}$ values. Both the formulation developed in Bou-Zeid et al. (2004) and the new formulation presented here were found to perform well in calculating blending heights and effective roughness lengths for momentum and heat. The effective roughness lengths calculated by the stability corrected model produced highly accurate average surface fluxes of momentum and heat when used with bulk similarity theory. The new model also calculates $z_{t,e}$ for each case, thus improving the estimation of the surface fluxes and the stability without the need to choose a function for $z_{t,e}$. For BZ04, reasonably accurate average fluxes are found when a correct single value of B^{-1} was specified. However, the ad hoc specification of a single B^{-1} value degrades surface-flux predictions for cases where the LES-determined B^{-1} is considerably higher or lower than the specified value.

Acknowledgments An allocation of computer time from the Center for High Performance Computing at the University of Utah is gratefully acknowledged.

References

Albertson JD, Parlange MB (1999a) Natural integration of scalar fluxes from complex terrain. Adv Water Res 23:239–252

Albertson JD, Parlange MB (1999b) Surface length scales and shear stress: implications for land–atmosphere interactions over complex terrain. Water Resour Res 35:2121–2132

Albertson JD, Kustas WP, Scanlon TM (2001) Large-eddy simulation over heterogeneous terrain with remotely sensed land surface conditions. Water Resour Res 37:1939–1953

Ament F, Simmer C (2006) Improved representation of land-surface heterogeneity in a non-hydrostatic numerical weather prediction model. Boundary-Layer Meteorol 121:153–174. doi:10.1007/s10546-006-9066-4

Andrén A, Brown AR, Graf J, Mason PJ, Moeng C-H, Nieuwstadt TM, Schumann U (1994) Large-eddy simulation of a neutrally stratified boundary layer: a comparison of four computer codes. Q J R Meteorol Soc 120:1457–1484

Arola A (1999) Parameterization of turbulent and mesoscale fluxes for heterogeneous surfaces. J Atmos Sci 56:584–598

Arya SP (2001) Introduction to micrometeorology, 2nd edn. Academic Press, San Diego, p 420

Avissar R, Pielke RA (1989) A parameterization of heterogeneous land surfaces for atmospheric numerical models and its impact on regional meteorology. Mon Weather Rev 117:2113–2136

Avissar R, Schmidt T (1998) An evaluation of the scale at which ground-surface heat flux patchiness affects the convective boundary layer using large-eddy simulations. J Atmos Sci 55:2666–2689
Beare RJ, MacVean MK (2004) Resolution sensitivity and scaling of large-eddy simulations of the stable boundary layer. Boundary-Layer Meteorol 112:257–281
Beare RJ, MacVean MK, Holtslag AAM, Cuxart J, Esau I, Golaz JC, Jimenez MA, Khairoutdinov M, Kosovic B, Lewellen D, Lund TS, Lundquist JK, McCabe A, Moene AF, Noh Y, Raasch S, Sullivan P (2006) An intercomparison of large-eddy simulations of the stable boundary layer. Boundary-Layer Meteorol 118:247–272. doi:10.1007/s10546-004-2820-6
Beljaars ACM, Holtslag AAM (1991) Flux parameterization over land surfaces for atmospheric models. J Appl Meteorol 30:327–341
Blyth EM (1995) Using a simple SVAT scheme to describe the effect of scale on aggregation. Boundary-Layer Meteorol 72:267–285
Blyth EM, Dolman AJ, Wood N (1993) Effective resistance to sensible- and latent-heat flux in heterogeneous terrain. Q J R Meteorol Soc 119:423–442
Bou-Zeid E, Meneveau C, Parlange MB (2004) Large-eddy simulation of neutral atmospheric boundary layer flow over heterogeneous surfaces: blending height and effective surface roughness. Water Resour Res 40:1–18
Bou-Zeid E, Parlange MB, Meneveau C (2007) On the parameterization of surface roughness at regional scales. J Atmos Sci 64:216–227
Brutsaert WH (1982) Evaporation into the atmosphere. Reidel, Dordrecht, p 316
Brutsaert WH (1998) Land-surface water vapor and sensible heat flux: spatial variability, homogeneity, and measurement scales. Water Resour Res 34:2433–2442
Businger JA, Wyngaard JC, Izumi Y, Bradley EF (1971) Flux–profile relationships in the atmospheric surface layer. J Atmos Sci 28:181–189
Canuto C, Hussaini MY, Qaurteroni A, Zang TA (1988) Spectral methods in fluid dynamics. Springer, New York, 584 pp
Chamberlain A (1966) Transport of gases to and from grass and grass-like surfaces. In: Proceedings of the Royal Society of London. Series A, Mathematical and Physical Sciences, vol 290. The Royal Society, London, pp 236–265
Claussen M (1990) Area-averaging of surface fluxes in a neutrally stratified, horizontally inhomogeneous atmospheric boundary layer. Atmos Environ 24A(6):1349–1360
Claussen M (1991) Estimation of areally-averaged surface fluxes. Boundary-Layer Meteorol 54:387–410
Delage Y (1997) Parameterising sub-grid scale vertical transport in atmospheric models under statically stable conditions. Boundary-Layer Meteorol 82:23–48
Derbyshire SH (1995) Stable boundary layers: observations, models and variability part I: modelling and measurements. Boundary-Layer Meteorol 74:19–54
Dyer AJ (1974) A review of flux–profile relationships. Boundary-Layer Meteorol 7:363–372
Fernando H, Well J (2010) Wither the stable boundary layer. Bull Am Meteorol Soc 91:1475–1484
Garratt JR (1990) The internal boundary layer—a review. Boundary-Layer Meteorol 50:171–203
Garratt JR (1992) The atmospheric boundary layer. Cambridge University Press, Cambridge, p 336
Garratt JR, Hicks BB (1973) Momentum, heat and water vapour transfer to and from natural and artificial surfaces. Q J R Meteorol Soc 99:680–687
Glendening JW, Lin CL (2002) Large eddy simulation of internal boundary layers created by a change in surface roughness. J Atmos Sci 59:1697–1711
Goode K, Belcher SE (1999) On the parameterization of the effective roughness length for momentum transfer over heterogeneous terrain. Boundary-Layer Meteorol 93:133–154
Grachev AA, Fairall CW, Persson POG, Andreas EL, Guest PS (2005) Stable boundary-layer scaling regimes: the SHEBA data. Boundary-Layer Meteorol 116:201–235
Holtslag B (2006) GEWEX atmospheric boundary-layer study (GABLS) on stable boundary layers. Boundary-Layer Meteorol. doi:10.1007/s10546-005-9008-6
Hopwood WP (1995) Surface transfer of heat and momentum over an inhomogeneous vegetated land surface. Q J R Meteorol Soc 121:1549–1574
Huang HY, Margulis SA (2010) Evaluation of a fully coupled large-eddy simulation-land surface model and its diagnosis of land-atmosphere feedback. Water Resour Res 46: W06512
King JC, Connolley WM, Derbyshire SH (2001) Sensitivity of modelled Antarctic climate to surface and boundary-layer flux parametrizations. Q J R Meteorol Soc 127:779–794
King JC, Jrrar A, Connolley WM (2007) Sensitivity of modelled atmospheric circulation to the representation of stable boundary layer processes. J Geophys Res Lett 34:L06708
Kosovic B, Curry JA (2000) A large eddy simulation study of a quasi-steady, stably stratified atmospheric boundary layer. J Atmos Sci 57:1052–1068

Lin CL, Glendening JW (2002) Large eddy simulation of an inhomogeneous atmospheric boundary layer under neutral conditions. J Atmos Sci 59:2479–2497
Mahrt L (1987) Grid-averaged surface fluxes. Mon Weather Rev 115:1550–1560
Mahrt L (1996) The bulk aerodynamic formulation over heterogeneous surfaces. Boundary-Layer Meteorol 78:87–119
Mahrt L (1998) Stratified atmospheric boundary layers and breakdown of models. Theor Comput Fluid Dyn 11:263–279
Mahrt L (2000) Surface heterogeneity and vertical structure of the boundary layer. Boundary-Layer Meteorol 96:33–62
Mahrt L, Mills R (2009) Horizontal diffusion by submeso motions in the stable boundary layer. Environ Fluid Mech 9:443–456
Mason PJ (1988) The formation of areally-averaged roughness lengths. Q J R Meteorol Soc 114:399–420
McCabe A, Brown AR (2007) The role of surface heterogeneity in modelling the stable boundary layer. Boundary-Layer Meteorol. doi:10.1007/s10546-006-9119-8
Monin AS, Obukhov AM (1954) Basic laws of turbulent mixing in the ground layer of the atmosphere. Trans Geophys Inst Akad Nauk USSR 151:163–187
Nieuwstadt FTM (1984) The turbulent structure of the stable, nocturnal boundary layer. J Atmos Sci 41(14):2202–2216
Nieuwstadt FTM (1985) A model for the stationary, stable boundary layer. In: Hunt JCR (ed) Proceedings of IMA conference on turbulence and diffusion in stable environments, Cambridge, pp 149–179
Orszag SA, Pao YH (1974) Numerical computation of turbulent shear flows. Adv Geophys 18A:224–236
Owen PR, Thomson WR (1963) Heat transfer across rough surfaces. J Fluid Mech 15(3):321–334
Patton EG, Sullivan PP, Moeng CH (2005) The influence of idealized heterogeneity on wet and dry planetary boundary layers coupled to the land surface. J Atmos Sci 62:2078–2097
Roy SB, Avissar R (2000) Scales of response of the convective boundary layer to land-surface heterogeneity. J Geophys Res Lett 27(4):533–536
Schmid HP, Bünzli B (1995) The influence of surface texture on the effective roughness length. Q J R Meteorol Soc 121:1–21
Stoll R, Porté-Agel F (2006a) Dynamic subgrid-scale models for momentum and scalar fluxes in large-eddy simulations of neutrally stratified atmospheric boundary layers over heterogeneous terrain. Water Resour Res 42:W01409
Stoll R, Porté-Agel F (2006b) Effect of roughness on surface boundary conditions for large-eddy simulation. Boundary-Layer Meteorol 118:169–187
Stoll R, Porté-Agel F (2008) Large-eddy simulation of the stable atmospheric boundary layer using dynamic models with different averaging schemes. Boundary-Layer Meteorol 126:1–28
Stoll R, Porté-Agel F (2009) Surface heterogeneity effects on regional-scale fluxes in stable boundary layers: surface temperature transitions. J Atmos Sci 66:412–431
Taylor PA (1987) Comments and further analysis on effective roughness lengths for use in numerical three-dimensional models. Boundary-Layer Meteorol 39(4):403–418
Thom AS (1972) Momentum, mass and heat exchange of vegetation. Q J R Meteorol Soc 98:124–134
Viterbo P, Beljaars A, Mahfouf JF (1999) The representation of soil moisture freezing and its impact on the stable boundary layer. Q J R Meteorol Soc 125(559):2401–2426
Wieringa J (1986) Roughness-dependent geographical interpolation of surface wind speed averages. Q J R Meteorol Soc 112:867–889
Wood DH (1982) Internal boundary layer growth following a step change in surface roughness. Boundary-Layer Meteorol 22:241–244
Wood N, Mason P (1991) The influence of static stability on the effective roughness lengths for momentum and heat transfer. Q J R Meteorol Soc 117:1025–1056